Published in final edited form as:
Cell Physiol Biochem. 2012 ; 30(1): 33–48. doi:10.1159/000339047.

Inhibition of Na^+-K^+-$2Cl^-$ cotransporter isoform 1 accelerates temozolomide-mediated apoptosis in glioblastoma cancer cells

Jehad Algharabli[2], **Douglas B. Kintner**[2], **Qiwei Wang**[3], **Gulnaz Begum**[1], **Paul A. Clark**[2], **Sung-Sen Yang**[4], **Shih-Hua Lin**[4], **Kristopher T. Kahle**[5], **John S. Kuo**[2], and **Dandan Sun**[1,2]

[1]Dept. of Neurology, Univ. of Pittsburgh, Pittsburgh, PA

[2]Dept. of Neurosurgery, Univ. of Wisconsin School of Medicine and Public Health

[3]Cellular and Molecular Pathology Training Program, Univ. of Wisconsin School of Medicine and Public Health

[4]Division of Nephrology, Dept. of Medicine, Tri-Service General Hospital, National Defense Medical Center, Taipei, Taiwan

[5]Dept. of Neurosurgery, Massachusetts General Hospital and Harvard Medical School, Boston, MA, USA

Abstract

The hallmark of apoptosis is a significant reduction in cell volume (AVD) resulting from loss of K^+_i and Cl^-_i. Loss of cell volume and lowering of ionic strength of intracellular K^+ and Cl^- occur before any other detectable characteristics of apoptosis. In the present study, temozolomide (TMZ) triggered loss of K^+_i and Cl^-_i and AVD in primary glioblastoma multiforme (GBM) cancer cells (GC) and GC cancer stem cells (GSC). We hypothesize that Na^+-K^+-$2Cl^-$ cotransporter isoform 1 (NKCC1) counteracts AVD during apoptosis in GBM cancer cells by regulating cell volume and Cl^- homeostasis. NKCC1 protein was expressed in both GC and GSC and played an essential role in regulatory volume increase (RVI) in response to hypertonic cell shrinkage and isotonic cell shrinkage. Blocking NKCC1 activity with its potent inhibitor bumetanide abolished RVI. These cells maintained a basal $[Cl^-]_i$ (~ 68 mM) above the electrochemical equilibrium for Cl^-_i. NKCC1 also functioned to replenish Cl^-_i levels following the loss of Cl^-_i. TMZ-treated cells exhibited increased phosphorylation of NKCC1 and its up-stream novel Cl^-/volume-sensitive regulatory kinase WNK1. Inhibition of NKCC1 activity with bumetanide accelerated AVD, early apoptosis, as well as activation of caspase-3 and caspase-8. Taken together, this study strongly suggests that NKCC1 is an essential mechanism in GBM cells to maintain K^+, Cl^-, and volume homeostasis to counteract TMZ-induced loss of K^+, Cl^- and AVD. Therefore, blocking NKCC1 function augments TMZ-induced apoptosis in glioma cells.

Keywords

glioblastoma multiforme; apoptosis; caspase; apoptotic volume decrease; temozolomide; bumetanide

Address correspondence to: Dandan Sun, M.D., Ph.D., Department of Neurology, University of Pittsburgh Medical School, S-598 South Biomedical Science Tower (BST), 3500 Terrace St., Pittsburgh, PA 15213, Phone: (412) 624-0418, FAX: (412) 648-3321, sund@upmc.edu.

INTRODUCTION

Glioblastoma multiforme (GBM) is a World Health Organization Grade IV cancer, the most malignant category of glial tumors with median survival time of less than one year [1–3]. Current standard therapies for GBM include surgical resection, radiation, and chemotherapy. The combined temozolomide (TMZ)-mediated chemotherapy and radiotherapy only modestly improve survival of GBM patients [2-yr survival rate of 27% [4]. The key challenge in the radio-chemotherapy treatment is an increase of a subpopulation of GBM cancer cells which are resistant to apoptosis. Therapeutic resistance has been suggested, in part, to result from an overexpression of drug transporters, enhanced DNA repair mechanisms against TMZ-induced apoptosis, and/or a subpopulation of drug-resistant glioma cancer stem cells [2,5].

TMZ causes a DNA O^6-methylguanine lesion which triggers DNA repair, depletes the enzyme O^6-methylguanine methyltransferase (MGMT), and leads to apoptotic cell death via extrinsic and/or intrinsic pathways [6]. The hallmark of apoptosis is a significant reduction in cell volume (AVD) resulting from loss of K^+_i and Cl^-_i [7,8]. AVD is an ubiquitous characteristic of apoptosis which is independent of the death stimuli [9,10]. Loss of cell volume and reduction of total intracellular ionic strength (via loss of K^+ and Cl^-) occur before any other detectable characteristics of apoptosis [11]. The reduction of intracellular ionic strength has been suggested to play a permissive role in activation of caspases and triggering the entire caspase cascade and apoptotic machinery [8]. However, it remains unknown whether TMZ triggers loss of K^+_i and Cl^-_i and AVD in glioma cells.

Normally, cells respond to volume perturbations by activating volume regulatory mechanisms such as regulatory volume increase (RVI), the process by which shrunken cells return to normal volume. RVI can only be mediated by the gain of osmotically active solutes such as Na^+, K^+, and Cl^- [12]. Na^+-K^+-$2Cl^-$ cotransporter isoform 1 (NKCC1), which transports 1 Na^+, 1 K^+ and 2 Cl^- ions into the cell under normal physiological conditions, is the primary cell volume regulatory protein in RVI in response to either hypertonic or isotonic cell shrinkage [12,13]. Therefore, we hypothesize that NKCC1 may counteract AVD during apoptosis in GBM cancer cells by regulating cell volume and Cl^- homeostasis. This study will shed light on whether a combined TMZ-based therapy with NKCC1 inhibition could present a novel therapeutic strategy, which may increase the efficiency of the current chemotherapy.

In the present study, we found that NKCC1 is the most important ion transport mechanism in the regulation of Cl^-_i and RVI in primary GBM cancer (GC) and cancer stem cells (GSC). Moreover, we detected that TMZ not only triggered AVD and loss of K^+_i and Cl^-_i during early apoptosis, but also concurrently stimulated NKCC1 and WNK1 activity in GC and GSC. Interestingly, pharmacological blockade of NKCC1 activity with its potent inhibitor bumetanide (BMT) enhanced TMZ-mediated apoptosis in GC and GSC. We conclude that BMT augments TMZ-induced apoptosis due to failure of compensatory entry of K^+ and Cl^-.

MATERIAL AND METHODS

Materials

Poly-L Lysine (PLL), laminin, heparin, human recombinant epidermal growth factor (EGF), gramicidin, nigericin, tributyltin, valinomcycin, propidium idodide (PI), TMZ, staurosporine (STS), and BMT were purchased from Sigma Chemicals (St. Louis, MO). Dulbecco's Modified Eagle Medium (DMEM), Ham's F12 medium, B27 supplement (without vitamin A), goat anti-IgG secondary antibodies Alexa Fluor® 488, PBFI-AM, calcein-AM, MQAE, and pluronic acid were obtained from Invitrogen (Carlsbad, CA). Human recombinant basal

fibroblast growth factor (bFGF), mouse/rat WNK1 affinity purified antibody, and human phospho-WNK1 (T60) affinity purified antibody were from R&D Systems (Minneapolis, MN). Accutase was from Millipore (Billerica, MA). Annexin V-FITC Apoptosis Kit was from Imgenex (San Diego, CA). NKCC (T4) antibody was from Developmental Studies Hybridoma Bank (Iowa City, IA). Caspase-3 antibody, caspase-8, and α-tubulin antibodies were from Cell Signaling (Beverly, MA). NKCC (R5) antibody against phosphorylated NKCC (*p*-NKCC) was a kind gift from Dr. Biff Forbush (Yale University).

Cell cultures

Glioblastoma cells (GC)—All studies involving human tissue were performed with approval from the University of Wisconsin-Madison Institutional Review Board with informed consent obtained from patients. Primary glioma cell lines (GC #22, #99) were established as described before [14]. Human glioblastoma multiforme cell line U87MG was obtained from the American Type Culture Collection (Manassas, VA). GC and U87MG were maintained in adherent cultures in plates coated with PLL and laminin in 90% DMEM supplemented with 10% FBS and PSA (100 units/ml penicillin, 100 μg/ml streptomycin, and 0.25 μg/ml amphotericin B). Cultures were passaged approximately every 4 days with fresh medium at a density of 10^5 cells/25cm^2 in a culture flask. Passages of 10–35 were used in this study.

GC cancer stem cells (GSC)—GSCs (#22 or #99) were isolated and characterized from the same GC line as previously reported [14]. GSC exhibited high CD133 expression, stem cell multipotency, and tumor initiation capability. Upon EGF and bFGF removal, GSC maintained sphere-forming and tumor initiation ability [14]. Cultures were passaged approximately every 7 days with 70% DMEM-high glucose and 30% Ham's F12 supplemented with B27, 5 μg/ml heparin, PSA, and EGF and bFGF (20 ng/ml each). To seed cells in plates coated with PLL and laminin, GSC spheres were incubated in accutase for 5 min at 37°C and dissociated with a P200 pipette. Cells were seeded at 10^5 cells/25cm^2 in culture flasks. Passages of 20–50 were used in this study.

Cell volume measurement

Cell volume change was determined using calcein as a marker of intracellular water volume, which was established previously [15]. Briefly, cells on coverslips were incubated with 0.5 μM calcein-AM for 30 min at 37°C. The cells were placed in a heated (37°C) imaging chamber (Warner Instruments, Hamden, CT) on a Nikon Ti Eclipse inverted epifluorescence microscope equipped with perfect focus, a 40X Super Fluor oil immersion objective lens, and a Princeton Instruments MicroMax CCD camera. Calcein fluorescence was monitored using a FITC filter set (excitation 480 nm, emission 535 nm, Chroma Technology, Rockingham, VT). Images were collected every 60 sec with MetaFluor image-acquisition software (Molecular Devices, Sunnyvale, CA). Regions of interest (0.5 μm in diameter) were selected in the cytoplasm of ~20 cells. Baseline drift resulting from photobleaching and dye leakage was corrected as described before [15]. The fluorescence change was plotted as a function of the reciprocal of the relative osmotic pressure and the resulting calibration curve applied to all subsequent experiments as described before [15]. The HEPES buffered isotonic solution contained (in mM, pH 7.4): 100 NaCl, 5.4 KCl, 1.3 $CaCl_2$, 0.8 $MgSO_4$, 20 HEPES, 5.5 glucose, 0.4 $NaHC0_3$, and 70 sucrose with 310 mOsm determined using an osmometer (Advanced Instruments, Norwood, MA). Anisosmotic solutions (240, 370, and 400 mOsm) were prepared by removal or addition of sucrose to the above solution.

Intracellular Cl^- concentration ($[Cl^-]_i$) measurement

The fluorescent dye MQAE was used to determine $[Cl^-]_i$ as described by Rocha-Gonzalez [16] with some modifications. Cells were incubated with 5 mM MQAE for 1–2 h (37°C) in a HEPES buffered isotonic solution. The coverslip was placed in the heated imaging chamber for 30 min before imaging. Using the Nikon Ti Eclipse inverted epifluorescence microscope and the 40X oil immersion objective lens, cells were excited every 60 sec at 340 nm and emission fluorescence at 460 nm recorded. Images were collected and analyzed with the MetaFluor image-processing software.

The fluorescence in MQAE-loaded cells drifted over time as a function of exposure to excitation light [16] and the drift in MQAE florescence was corrected by a linear fit. At the end of each experiment, the MQAE florescence was calibrated under a steady state condition when $[Cl^-]_o$ and $[Cl^-]_i$ were considered equal by exposing cells to a series of calibration solutions containing 10 μM tributylin and 5 μM nigericin [16]. The series of Cl^- calibration solutions contained (in mM): 1.27 $Ca(OH)_2$, 0.8 $MgSO_4$, 5 HEPES, 5.5 glucose, 120 K^+, and variable Cl^- and NO_3^-. In these solutions, Cl^- was varied from 0 to 60 mM keeping the sum of Cl^- and NO_3^- equal to 120 mM. KSCN (150 mM) was used to quench the MQAE fluorescence, which was taken as background fluorescence. $[Cl^-]_i$ was determined from the MQAE fluorescence (drift-corrected, background-corrected) using the following equation: $[Cl^-]_i = [(F_o/F_t)-1)]/Ksv$, where F_o was the fluorescence in 0 mM $[Cl^-]_o$, F_t was the fluorescence at any given time point, and K_{sv} was the slope of the linear fit of MQAE fluorescence vs. the $[Cl^-]_o$ of the standards. A K_{sv} of 13.4 ± 1.5 M^{-1} was calculated in our study, a value similar to that reported by others [16].

Intracellular K^+ ($[K^+]_i$) measurement

$[K^+]_i$ was determined by a modified method as described by Kiedrowski [17]. Briefly, cells were incubated with 5 μM PBFI-AM plus 0.02 % pluronic acid at 37°C for 90 min. The coverslips were placed in the heated imaging chamber at 37°C. Cells were rinsed and images collected using the Nikon Ti Eclipse inverted epifluorescence microscope equipped with the 40X oil immersion objective lens. Cells were excited every 20 sec at 340 and 380 nm and the emission fluorescence at 510 nm recorded. Images were analyzed with the MetaFluor image-processing software. At the end of each experiment, a calibration was performed by exposing cells to standards of varying K^+ concentrations plus gramicidin and valinomcycin (10 μM each). K^+ standards contained 30 mM NaCl, 20 mM HEPES, and 1 mM $MgCl_2$. K^+ was varied from 20 to 100 mM by substituting K^+-gluconate and LiCl such that the sum of K^+ and Li^+ was 100 mM.

Quantification of apoptosis with live cell imaging

Cells were incubated either with TMZ (0 – 500 μM) or TMZ plus 10 μM BMT for 48 h. To determine apoptotic cell damage, cells were rinsed with ice-cold PBS and incubated for 30 min at RT with 100 μl binding buffer, 5 μl FITC Annexin-V, and 5 μl propidium iodide (PI) provided in the Annexin V-FITC Apoptosis Kit. Brightfield, FITC (Annexin-V), and Texas Red (PI) images were collected from 4 random fields in each well using the Nikon Ti Eclipse microscope and a 20X objective. The total number of cells in each field was counted in the brightfield image. Apoptotic cells were calculated as the percentage of the Annexin V^+/PI^- cells.

We found that 500 μM TMZ led to robust apoptotic volume decrease and early apoptosis in a very short time (1–4 hours). This raised concerns about the impact of cell volume change and cell membrane damage on dye retention in TMZ-treated cells in live cell imaging studies (cell volume, K^+, and Cl^-) and of detached cells on sample collection for

immunoblotting assays. Therefore, for these studies, we reduced TMZ concentration to 100 μM.

Flow cytometry assay for apoptosis

Assays were carried out by using an Annexin V-FITC Apoptosis Kit. Cultures were treated with a control medium or a medium containing 10 μM BMT, 500 μM TMZ, or 500 μM TMZ plus 10 μM BMT for 4 h. STS (4 μM, 4 h) was used as a positive control. Cultures were rinsed with ice-cold phosphate-buffered saline (PBS; pH 7.4) and incubated with accutase (2 ml per 25 cm^2 surface area) at 37°C for 5 min. The detached cells (from PBS wash as well as from accutase treatment) were collected by centrifugation (500×g, 10 min). The combined cell pellets were washed with PBS and resuspended in 100 μl binding buffer. Cells were incubated with 5 μl FITC Annexin-V and 5 μl PI in dark at RT for 20 min. After incubation, 400 μl binding buffer was added to each sample. Cells were analyzed using a Becton Dickinson Biosciences FACSCalibur (BD Biosciences, CA). Early apoptotic cells were determined as Annexin V-positive and PI-negative cells (Annexin V^+/PI^-).

Changes in cell size were also evaluated by forward light scattering vs. side light scattering 3D plots using Becton Dickinson Biosciences FACSCalibur and CellQuest software. Decrease in the forward light scattering values of the cells reflected a decrease in cell size.

Time-lapse assay for apoptotic volume decrease

Cultures in 35 mm glass bottom culture dishes were placed in a stage top incubator (Tokai Hit, Shizuoka-ken, Japan) at 37°C and 5% CO_2. Cultures were treated with a control medium or a medium containing 500 μM TMZ, or 500 μM TMZ plus 10 μM BMT for 12 h. Time-lapse DIC images were collected every 15 min for 12 h using the Nikon Ti Eclipse microscope with perfect focus. The surface area of each cell was manually traced using MetaMorph (Molecular Devices, CA). 5 cells in each field were selected and their surface areas determined. Cell surface area values at each time were normalized to the corresponding values at time 0 h. Mean cell surface area (± SEM) for each time point was calculated by averaging the normalized areas of cells for each hour.

Immunoblotting assay

Cells were washed with ice-cold PBS that contained 2 mM EDTA and protease inhibitors as described before [18]. Cells were lysed by sonication at 4°C. Protein content of the cellular lysate was determined with BCA Protein Assay Kit (Pierce, Rockford, IL). Samples and prestained molecular mass markers (Bio-Rad, Hercules, CA) were denatured in SDS reducing buffer (1:2 vol/vol) and heated at 90°C for 5 min. The samples were then electrophoretically separated on 10–15% SDS gels. After transferring to PVDF membranes, the blots were blocked in 7.5% nonfat dry milk in Tris buffered saline for 1 h at RT and then incubated with a primary antibody at 4°C overnight. The blots were probed with monoclonal T4 antibody against total NKCC1 (1:2000), polyclonal antibody (R5) against a diphosphopeptide containing T184 and T189 of shark NKCC1 (*p*-NKCC; 1:1000, [19]), polyclonal antibodies against total WNK1 (1:1000), polyclonal rabbit anti-phospho-WNK1 antibody (*p*-WNK1; 1:2000), polyclonal anti-caspase-3 (full length and large fragment of cleaved caspase-3; 1:1000), monoclonal anti-caspase-8 (full length, cleaved intermediate p43/41 and active capspase-8 fragment p18; 1:500), or monoclonal alpha tubulin antibody. After rinsing, the blots were incubated with horseradish peroxidase-conjugated secondary IgG for 1 h at RT. Bound antibody was visualized with an enhanced chemiluminescence assay (Amersham, Piscataway, NJ).

Cell proliferation analysis

Cell proliferation analysis was performed using CellTiter 96® AQ_{ueous} One Solution Cell Proliferation Assay kit [MTS; 3-(4, 5-dimethylthiazol-2-yl)-5-(3-carboxymethoxyphenyl)-2-(4-sulfophenyl)-2H-tetrazolium] (Promega, Madison, WI). Cells were treated with vehicle (DMSO), 10 μM BMT, 250 μM TMZ, or 250 μM TMZ + 10 μM BMT for 0, 24, and 48 h, respectively. 20 μl of CellTiter 96® AQ_{ueous} One Solution Reagent was added into each well of a 96-well plate (5,000 cells/100 μl medium). After 1 h incubation, the absorbance of each well at 490 nm was determined with a microplate reader (Molecular Devices, Sunnyvale, CA). The background absorbance was subtracted from all readings. Data are expressed as relative MTS activity.

Cell cycle analysis

Monolayer cell cultures were rinsed with PBS and the medium collected (to harvest floating cells). After trypsinization, detached cells and floating cells were combined and fixed by slow addition of ice-cold 70% (v/v) ethanol and stored at 4°C for 1 h. The fixed cells were then pelleted (500×g, 20 min), and washed twice in PBS. The cells were incubated with 20 μg /ml PI in PBS containing 100 μg /ml ribonuclease A at 37°C for 30 min in the dark. Cell cycle distribution was analyzed by Becton Dickinson Biosciences FACSCalibur and ModFit LT^{TM} software with 20, 000 events per determination. The amount of DNA is proportional to the amount of PI dye staining. DNA content in each phase of the cell cycle (G1, S and G2/M) was calculated with ModFit LT^{TM} software.

Statistics

Statistical significance was determined by student's *t*-test or an ANOVA (Bonferroni post-hoc test) in the case of multiple comparisons. A P-value < 0.05 was considered statistically significant. N values represent the number of cultures used in each experiment.

RESULTS

NKCC1-mediated regulatory volume increase (RVI) response in GC and GSC

The expression of NKCC1 protein in GC and GSC was confirmed by immunofluorescence staining as well as immunoblotting (data not shown). Because a high degree of heterogeneity is characteristic of GBM, multiple primary cell lines were examined in this study. We measured NKCC1-mediated RVI in GC (#22, 99) and GSC (#22, 99). As shown in Figure 1, exposing these cells to a hypertonic HEPES-MEM (370 mOsm) buffer induced cell shrinkage in 2–3 min ranging from 20 to 25% (Figure 1 A–D). No RVI response was detected within 10 min of hypertonic exposure. Cell volume started recovering in these cells after 10–15 min at a rate of 1.4–2.6% vol/min. Within 25 min of hypertonic exposure, all cell types regulated their volume back to the original control levels (Figure 1 A–D). In contrast, blocking NKCC1 activity with its potent inhibitor BMT (10 μM) abolished RVI in all cell lines (Figure 1 A–D). BMT at a low concentration (< 10 μM) specifically inhibits NKCC1 activity [IC_{50} of 0.1 μM, [13]], which has been validated in previous studies from our lab and others [20,21]. Taken together, our data demonstrate that NKCC1-mediated RVI is essential in regulating cell volume homeostasis in response to osmotic stress in both GC and GSC cell types.

The BMT-treated primary glioma cells were able to restore cell volume upon returning them to the isotonic solution. This is consistent with our previous study in NKCC1 null cells ($NKCC1^{-/-}$) [20]. This is because a shrunken cell has greater osmotic pressure when placed in an isotonic solution and recovers its volume via rapid inward water movement.

TMZ induced a loss of K^+_i and Cl^- in GC and GSC

As shown in Figure 2 A, B, 4 h of TMZ treatment (100 μM) led to 27% loss in $[K^+]_i$ and a ~ 34% reduction in $[Cl^-]_i$ in GC (#22). Inhibition of NKCC1 activity with BMT (10 μM) further lowered $[K^+]_i$ by 45% and $[Cl^-]_i$ by ~ 62%. Figure 2 C illustrates that NKCC1 played an essential role in replenishing Cl^-_i in control as well as in TMZ-treated cells after loss of $[Cl^-]_i$. When NKCC1 was blocked with BMT for 2 h (Con) or during 4 h of TMZ treatment, Cl^-_i uptake was abolished. More importantly, effects of TMZ on Cl^- uptake rate were determined by calculating $[Cl^-]_i$ by fitting a slope to the last point of 0 mM extracellular Cl^-_o and the first point following the reintroduction of Cl^-. Cl^- uptake rate appeared to be increased ($p < 0.05$, Figure 2 C, **upper panels**). Since the rate of Cl^- uptake was very fast, we conducted additional experiments and collected Cl^- data every 10 sec when Cl^-_o was reintroduced (Figure 2 C, **lower panels**). By fitting a slope to the last point of 0 mM extracellular Cl^-_o and the first point following reintroduction of Cl^-_o, the Cl^- uptake rate was increased from a control level of 57 ± 2 mM/min to 142 ± 34 mM/min in TMZ-treated cells, (**$p < 0.05$**, Figure 2 C, **lower panel**). Interestingly, blocking NKCC1 activity with BMT completely abolished the Cl^- uptake in the TMZ-treated cells. These data suggest that NKCC1 plays a role in regulation of intracellular Cl^- in control and TMZ-treated glioma. However, given the fast kinetics of Cl^- uptake after the reintroduction of Cl^-_o, the MQAE dye method is not optimal in determining changes in Cl^- uptake rates.

NKCC1-mediated RVI remains active in the TMZ-treated cells

We further tested whether NKCC1-mediated RVI was altered during TMZ-mediated apoptosis. Figure 2 D shows that RVI slowed down in the TMZ-treated GC (#22), but remained sensitive to NKCC1 blockade. NKCC1-mediated RVI was reduced by ~ 50% in the TMZ-treated GC (data not shown). In contrast, TMZ did not have any inhibitory effects on RVI in GSC (Figure 2 D). These data clearly imply that NKCC1 remains active in both GC and GSC after TMZ treatment, which may allow these cells to counteract the TMZ-induced AVD and increase their resistance to TMZ-mediated apoptosis.

Inhibition of NKCC1 activity accelerates TMZ-induced AVD

We further investigated the role of NKCC1 in counteracting AVD and apoptosis. Cell volume was monitored with the time-lapse microscopy. GSC (#22) was treated with TMZ (500 μM) for 12 h. Cell volume changes were monitored with the time-lapse microscopy. As shown in Figure 3 A, B, TMZ exposure triggered AVD in GSC at 6 – 12 h. 8 h of TMZ exposure reduced GSC volume by 38 ± 7%. No further cell shrinkage developed during 8–12 h of TMZ exposure. In contrast, a combined treatment with BMT (10 μM) accelerated the TMZ-induced AVD process (arrowhead, Figure 3 A). Under these conditions, GSC exhibited reduction of cell volume as early as at 1 h (Figure 3 B). It only took 4 h to trigger 20% AVD in these cells ($p < 0.05$). GSC lost its volume by 49 ± 6% at 12 h in the presence of TMZ plus BMT. These data strongly suggest that blocking NKCC1 activity accelerated TMZ-mediated AVD in GSC. The BMT alone treatment was performed and there were no significant effects on cell volume (data not shown). In addition, Figure 3 C shows flow cytometry analysis of cell size changes based on the forward scatter vs. side scatter of light. Control GC (#22) exhibited a small population of shrunken cells (18.2 ± 4.1%). TMZ plus BMT (4 h) caused a significant increase in the population of GC with a decreased forward scatter and increased side scatter of light (30.3 ± 0.7%, $p < 0.05$ vs. Con), which indicates shrunken cells, whereas GC treated with either BMT or TMZ alone did not show significant increase of shrunken population than control ($p > 0.05$ vs. Con). In a positive control study, staurosporine (STS)-treated GC also exhibited an increase in cell shrinkage (48.4 ± 6.7%, $p < 0.05$ vs. Con). Taken together, this study clearly demonstrates that blocking NKCC1 activity sensitized GSC and GC to TMZ-mediated AVD.

Cell shrinkage triggers activation of WNK/NKCC1 pathways

It is established that hypertonic cell shrinkage triggers phosphorylation of NKCC1 at the conserved regulatory locus (Thr^{184} and Thr^{189} of shark NKCC1) of the N terminus and stimulates NKCC1 activity [19]. We further investigated cellular mechanisms underlying regulation of NKCC1 in GC (#22). As shown in Figure 4 A, C, exposing GC to hypertonic HEPES-MEM (370 mOsm) for 20 min led to an increase in *p*-NKCC1 protein expression. Concurrently, an up-regulation of Cl^-/volume-sensitive kinase *p*-WNK1 was also detected in GC in response to hypertonic shrinkage (Figure 4 B, D). Osmotic cell shrinkage stimulated expression of both phosphorylated and non-phosphorylated NKCC1 and WNK1 (Figure 4 C, D). These findings suggest that WNK-mediated signal transduction pathways may play a role in regulation of NKCC1 phosphorylation in GC.

Interestingly, TMZ (100 μM, 4 h) triggered an up-regulation of *p*-NKCC1 and *p*-WNK1 in GC (#22). The level of *p*-NKCC1 and *p*-WNK1 remained elevated in the presence of TMZ plus BMT (Figure 4 E–H). Taken together, the data show that TMZ treatment stimulated WNK-mediated regulation of NKCC1 in GC.

BMT augments TMZ-mediated apoptosis due to failure of K^+ and Cl^- entry

We hypothesized that NKCC1 counteracts TMZ-induced loss of K^+ and Cl^- and prolongs cell survival following the TMZ-induced apoptosis. To test this further, we investigated whether blocking NKCC1 would sensitize GC to TMZ-induced apoptosis. Early apoptosis was determined in cells with Annexin V^+/PI^- staining. As shown in Figure 5 A, low levels of early apoptotic cells were detected in control or BMT-treated GC (#22). Either TMZ (500 μM, 4 h) or STS (4 μM, 4 h) induced a significant increase in early apoptotic cells. Moreover, blocking NKCC1 activity in the TMZ-treated cells triggered the highest level of apoptosis ($p < 0.05$, TMZ vs. TMZ plus BMT). Most importantly, there was a positive correlation between cell shrinkage and early apoptosis with a Pearson coefficient value of 0.99 ($p < 0.01$, $n = 3$).

We further examined whether inhibition of NKCC1 can enhance TMZ-mediated activation of down-stream apoptotic pathways including extrinsic apoptotic pathway initiator caspase-8 and executioner caspase-3. GC were exposed to 10 μM BMT, 100 μM TMZ, or TMZ plus BMT. Time-dependent cleavage of caspase-3 and caspase-8 was evaluated at 4, 48, or 96 h. As shown in Figure 5 B, C, neither BMT nor TMZ alone had a significant effect on caspase-3 and caspase-8 activation. In contrast, TMZ plus BMT accelerated activation of caspase-3 and caspase-8, as reflected by the significantly cleaved caspase-3 (p17) and caspase-8 (p18) after 48 h and 96 h treatment. STS (4 μM for 4 h) served as a positive control for activation of caspase-3 and caspase-8. Taken together, these results indicate that blocking NKCC1 activity enhances TMZ-mediated apoptosis in GC. This conclusion is further supported by our findings that inhibition of NKCC1 activity enhanced Annexin V staining signals at 48 h in the dose range of 100–500 μM (Figure 5 D). Figure 5 D clearly illustrates that this phenomenon was consistent in all four different GBM cell lines (primary GC lines #22 and #99, primary GSC #99, and U87MG).

Moreover, during 48 h exposure to TMZ, cell proliferation in these different GBM cell lines was not significantly reduced, either in the presence or absence of BMT (Figure 6 A). It has been established that TMZ causes G2/M arrest in the cell cycle [22]. As shown in Figure 6 B, C, BMT alone did not change cell cycle distribution of GC. TMZ treatment significantly reduced G1 phase cells and arrested GC in G2/M phase (Figure 6 B, C). G2/M arrest remained unchanged in the presence of TMZ + BMT. This further supports our conclusion that NKCC1 promtoes glioma cell survival via regulating ionic homeostasis.

DISCUSSION

NKCC1-mediated Cl^- accumulation in glioma cells

In the current study, NKCC1 protein expression was detected in GC and GSC. This is consistent with previous findings on abundant expression of NKCC1 protein in various gliomas [23,24]. We speculate that NKCC1 functions in accumulating Cl^-_i in GC and GSC. Using the Cl^--sensitive dye MQAE approach, we report here that both cell types had a basal level of $[Cl^-]_i$ (~ 70 mM), which is higher than anticipated by passive Cl^- distribution [25,26]. Inhibition of NKCC1 with BMT reduced the basal $[Cl^-]_i$ to ~ 30–40 mM in both GC and GSC, indicating that NKCC1 is required for the elevated basal $[Cl^-]_i$ in these cells. Moreover, NKCC1 also functions in replenishing Cl^- following loss of Cl^- after exposing cells to low Cl^-_o. Elevated $[Cl^-]_i$ between 80–100 mM has been reported in gliomas [23]. NKCC1 is also responsible for active accumulation of Cl^- in neural progenitor cells and immature neurons [26,27]. Our current study demonstrates that the high levels of $[Cl^-]_i$ in primary GBM cells are established by the function of NKCC1.

The NKCC1-mediated basal level “set-point” for $[Cl^-]_i$ (higher than the electrochemical equilibrium for Cl^-_i) is a prerequisite for channel-mediated Cl^- efflux in gliomas. The loss of Cl^- through Cl^- channels and subsequent isotonic cell shrinkage play an important role during glioma cell migration [23,24]. Pharmacological inhibition of NKCC1 activity reduces D54-MG cell migration in transwell apparatus and in xenographed tumor tissues [24]. The effect likely results from reducing the Cl^- gradient as well as Cl^- efflux upon Cl^- channel activation.

BMT accelerates AVD in TMZ-mediated apoptosis

We further characterized the function of NKCC1 in RVI in GC and GSC. Following hypertonic cell shrinkage, all cells exhibited RVI responses. Blocking NKCC1 activity with its potent inhibitor BMT abolished RVI in both GC and GSC. These findings suggest that NKCC1 plays an essential role in RVI in these cells. This is consistent with the established role of NKCC1 in RVI in many cell types via importing $1Na^+$, $1K^+$ and $2Cl^-$ ions into the cell [12,13]. ~ 30% tumor cells (GSC #22, #99 and GC #99) showed some degree of "post hyperosmotic" swelling (8–15%) due to entrance of water after switching the medium to isotonic medium. However, this phenomenon was lost when all data were averaged.

TMZ-induced DNA O^6-methylguanine lesion can induce apoptosis either via activating extrinsic apoptotic pathway or a mitochondria-dependent intrinsic pathway [6]. Apoptosis requires persistent cell shrinkage. AVD in part results from the loss of intracellular K^+ and Cl^- content and water [7,9]. The loss of K^+, Cl^- as well as Na^+_i results in an 80–85% loss of cell volume, DNA degradation, and apoptotic body formation in Jurkat cells [11]. We detected a decrease in K^+_i concentration in the TMZ-treated glioma, which is consistent with other reports [11]. Jurkat T-cells treated with Fas ligand for 4 h results in a decrease in K^+_i concentration from 140 mM to 30 mM along with a cell volume loss of 20–40% [11].

It has been well documented that diverse types of K^+ channels (voltage-gated or Ca^{2+}-dependent) are responsible for the efflux of K^+_i during apoptosis, in different cell types and in response to different apoptosis-inducing stimuli [28]. In human lens epithelial cells, 4-aminopyridine-sensitive voltage-gated K^+ channels are involved in loss of K^+_i, induction of AVD, and apoptosis [28]. Future studies are needed to investigate whether TMZ stimulates the voltage-gated or Ca^{2+}-dependent K^+ channels in these primary glioma cells.

In the TMZ-treated cells, we found that Cl^-_i was reduced, likely resulting from loss of Cl^- via the Cl^- channels. A parallel loss of K^+ and Cl^- occurred during apoptosis to maintain the electrochemical neutrality in cells [7]. Thus, inhibition of Cl^- channels reduces apoptosis

and blunts AVD [8]. Several types of Cl^- channels (ClC-2, ClC-3) have been shown to play a role in glioma [29]. Moreover, KCC (KCC1, KCC3a, and KCC4) expressed in glioma cell lines and primary glioma have been suggested to play a role in regulatory volume decrease [30,31]. It remains unexplored whether TMZ stimulates KCC activity in glioma and leads to a parallel loss of K^+ and Cl^-.

In the current study, we detected reduced K^+ and Cl^- concentrations in TMZ-treated primary glioma cells, which is different from an isosomotic reduction of K^+ and Cl^- in typical AVD. Several factors could contribute to the dilution of K^+ and Cl^- concentrations in the TMZ-treated cells, including NKCC1-mediated Na^+ entry along with water and Cl^- or reduction of water efflux-mediated by aquaporin proteins. The first possibility is supported by robust increase of NKCC1 protein expression and its elevated phosphorylation after TMZ treatment. The second possibility is supported by a report that aquaporin 4 (AQP4) protein was down-regulated in GBM tumor cells after combined chemotherapy and radiotherapy, which reduces peritumoural brain edema formation [32]. Collectively, these changes could lead to reduce K^+ and Cl^- concentrations in TMZ-treated primary glioma cells.

In GBM cells, TMZ triggered almost electroneutral loss of intracellular K^+ and Cl^-. However, in the presence of TMZ+BMT, there was more intracellular Cl^- loss than K^+ loss (45% K^+ vs. 65 % Cl^-). Given the stoichiometry of $1Na^+$, $1K^+$ and $2Cl^-$ ions for NKCC1, it is possible that blocking NKCC1 function by BMT and subsequent reduction of compensatory ion influx could have a more profound effect on Cl^-_i loss.

Function of RVI in apoptotic cells

It is poorly understood why the normal RVI mechanisms fail to regulate cell volume during persistent cell shrinkage in apoptosis. Numata et al. showed that no RVI was detected in HeLa cells following hypertonic shrinkage in the presence of STS [33]. Similar findings were found in anti-Fas ligand treated cells [9] and apoptotic HeLa cells triggered by STS [34]. In contrast, in the current study, we found that treatment of GSC with TMZ for 4 h did not significantly affect NKCC1-mediated RVI. The TMZ-treated GSC regulated its volume in response to osmotic stress similar to control GSC. Our study indicates that primary GBM gliomas regulate NKCC1 differently than other tumor cells. More importantly, we observed that inhibition of NKCC1 activity with BMT abolished RVI in TMZ-treated GC as well as GSC. Treating cells with BMT plus TMZ significantly accelerated AVD and increased apoptosis in gliomas (both GC and GSC). These findings suggest that NKCC1-mediated RVI remains functional and continues to regulate cell volume in the TMZ-treated gliomas. Thus, NKCC1 may play a crucial role to replenish K^+_i and Cl^-_i. Therefore, NKCC1-mediated regulation of K^+_i, Cl^-_i, and RVI can counteract AVD during TMZ-mediated apoptosis in glioblastoma cell lines.

Bortner et al. reported that there is an early reversal of K^+_i and Na^+ i gradients in apoptotic Jurkat T cells, which is important in triggering apoptosis [11]. It is in part a result of an impairment of Na^+/K^+ ATPase function [11]. Blocking of Na^+/K^+ ATPase with ouabain significantly enhances anti-Fas induced apoptosis in Jurkat cells and cortical neurons [35,36]. NKCC1 activity contributes to Na^+ accumulation in astrocytes and neurons [20,37]. Therefore, it is plausible that NKCC1 activation during TMZ-mediated apoptosis can enhance Na^+_i accumulation in gliomas.

Inhibition of NKCC1 activity sensitizes GC as well as GSC to TMZ-induced apoptosis

The novel Cl^-/volume-sensitive regulatory kinases WNK (with no K=lysine), a family of serine-threonine kinases, are activated by the loss of Cl^-_i and cell shrinkage [38,39]. WNK kinases stimulate NKCC1 activation by promoting net protein phosphorylation [40–42]. In

our study, we detected a concurrent increase in phosphorylation of NKCC1 as well as of WNK1 in TMZ-treated GC. We speculate that the increase in *p*-WNK1 expression likely results from TMZ-mediated loss of Cl^-_i and cell shrinkage because both changes were detected in glioma after 4 h of TMZ treatment. This further suggests that this evolutionarily-conserved WNK/NKCC1 signaling pathway plays a role in defending gliomas against cell volume and Cl^- dysregulation following TMZ treatment. Interestingly, we detected a significant elevation of total NKCC1 and WNK1 protein expression in glioma cells in response to 20-min hypertonic stress. The rapid upregulation of the two proteins likely results from de novo protein synthesis by using an existing pool of mRNA. Similarly, rapid increase in NKCC1 protein has been observed in the gills of Atlantic killifish when transferred from fresh to seawater [< 6 hours, [43]]. Therefore, the fast upregulation of transporter proteins and their regulatory kinases will allow cells to quickly acclimate to an altered osmotic environment.

It has been established that AVD precedes cytochrome c release, caspase-3 activation, and DNA laddering [7,28]. In the current study, we found that TMZ alone did not activate caspase-3 and caspase-8 after 48–96 h treatment. In contrast, TMZ plus BMT accelerated cleavage of caspase-3 and caspase-8 after 48–96 h treatment. This clearly indicates that BMT augments TMZ-induced apoptosis due to failure of compensatory K^+ and Cl^- entry. This phenomenon was consistent in all four GBM cell lines (primary GC #22, #99, GSC #99, and U87MG). It is established that TMZ causes G2/M arrest in the cell cycle [22] and reduces cell proliferation during 5–14 day exposure to TMZ [22,44,45]. In the current study, treatment of cells with TMZ for 48 h in the presence or absence of BMT did not alter cell proliferation. We anticipate that chronic exposure of cells to TMZ and BMT would reduce cell proliferation in light of its effects on cell cycle. Importantly, our data demonstrate that blocking of NKCC1 with BMT decreased the onset time for TMZ-mediated apoptosis.

In summary, we investigated the role of NKCC1 in regulation of K^+_i, Cl^-_i, as well as, cell volume homeostasis in gliomas. NKCC1 played an essential role in RVI in response to hypertonic cell shrinkage and isotonic cell shrinkage. NKCC1 also functioned in maintaining $[Cl^-]_i$, well above the electrochemical equilibrium for Cl^-. As summarized in Figure 7, NKCC1 activity in the TMZ-treated cells was stimulated via the novel Cl^-/volume-sensitive regulatory kinase WNK-mediated signaling transduction pathways. Most importantly, inhibition of NKCC1 activity accelerated TMZ-induced AVD and apoptosis. This led us to conclude that NKCC1 activation accumulates K^+_i and Cl^-_i to counteract AVD and restore intracellular ionic strength, reduce caspase-mediated apoptosis, and promote cell survival following TMZ-mediated DNA damage. Therefore, inhibition of NKCC1 protein can sensitize glioma to TMZ-mediated apoptosis. Our study suggests that a combined TMZ-based therapy with NKCC1 inhibition may present a novel therapeutic strategy to increase the efficiency of the current GBM chemotherapy.

Acknowledgments

This work was supported in part by NIH grant R01NS75995, R01NS38118, and R01NS42828 (D. Sun), NIH grant P30 HD03352 (Waisman Center), a NIH T32 grant to University of Wisconsin Stem Cell Training Program (P. A. Clark), and the HEADRUSH Brain Tumor Research Professorship, the AANS-NREF Young Clinician Investigator Award, Loff Memorial Fund, and Department of Neurological Surgery Brain Tumor Research Fund (J. S. K).

ABBREVIATIONS

AVD	apoptotic volume decrease
BMT	bumetanide

GBM	glioblastoma multiforme
GC	glioma cells
GSC	glioma stem cells
MGMT	O^6-methylguanine methyltransferase
NKCC1	Na^+-K^+-$2Cl^-$ cotransporter isoform 1
PI	propidium idodide
RVI	regulatory volume increase
STS	staurosporine
TMZ	temozolomide
WNK	kinase with no K=lysine

Reference List

1. Louis DN. Molecular pathology of malignant gliomas. Annu Rev Pathol. 2006; 1:97–117. [PubMed: 18039109]
2. Denysenko T, Gennero L, Roos MA, Melcarne A, Juenemann C, Faccani G, Morra I, Cavallo G, Reguzzi S, Pescarmona G, Ponzetto A. Glioblastoma cancer stem cells: heterogeneity, microenvironment and related therapeutic strategies. Cell Biochem Funct. 2010; 28:343–351. [PubMed: 20535838]
3. Dirks PB. Brain tumor stem cells: the cancer stem cell hypothesis writ large. Mol Oncol. 2010; 4:420–430. [PubMed: 20801091]
4. Stupp R, Mason WP, van den Bent MJ, Weller M, Fisher B, Taphoorn MJ, Belanger K, Brandes AA, Marosi C, Bogdahn U, Curschmann J, Janzer RC, Ludwin SK, Gorlia T, Allgeier A, Lacombe D, Cairncross JG, Eisenhauer E, Mirimanoff RO. Radiotherapy plus concomitant and adjuvant temozolomide for glioblastoma. N Engl J Med. 2005; 352:987–996. [PubMed: 15758009]
5. Liu G, Yuan X, Zeng Z, Tunici P, Ng H, Abdulkadir IR, Lu L, Irvin D, Black KL, Yu JS. Analysis of gene expression and chemoresistance of $CD133^+$ cancer stem cells in glioblastoma. Mol Cancer. 2006; 5:67. [PubMed: 17140455]
6. Roos WP, Batista LF, Naumann SC, Wick W, Weller M, Menck CF, Kaina B. Apoptosis in malignant glioma cells triggered by the temozolomide-induced DNA lesion O6-methylguanine. Oncogene. 2007; 26:186–197. [PubMed: 16819506]
7. Okada Y, Maeno E. Apoptosis, cell volume regulation and volume-regulatory chloride channels. Comp Biochem Physiol A Mol Integr Physiol. 2001; 130:377–383. [PubMed: 11913451]
8. Bortner CD, Cidlowski JA. Cell shrinkage and monovalent cation fluxes: role in apoptosis. Arch Biochem Biophys. 2007; 462:176–188. [PubMed: 17321483]
9. Bortner CD, Hughes FM Jr, Cidlowski JA. A primary role for K^+ and Na^+ efflux in the activation of apoptosis. J Biol Chem. 1997; 272:32436–32442. [PubMed: 9405453]
10. Maeno E, Ishizaki Y, Kanaseki T, Hazama A, Okada Y. Normotonic cell shrinkage because of disordered volume regulation is an early prerequisite to apoptosis. Proc Natl Acad Sci U S A. 2000; 97:9487–9492. [PubMed: 10900263]
11. Bortner CD, Sifre MI, Cidlowski JA. Cationic gradient reversal and cytoskeletonindependent volume regulatory pathways define an early stage of apoptosis. J Biol Chem. 2008; 283:7219–7229. [PubMed: 18187415]
12. Strange K. Cellular volume homeostasis. Adv Physiol Educ. 2004; 28:155–159. [PubMed: 15545344]
13. Russell JM. Sodium-potassium-chloride cotransport. Physiol Rev. 2000; 80:211–276. [PubMed: 10617769]

14. Clark PA, Treisman DM, Ebben J, Kuo JS. Developmental signaling pathways in brain tumor-derived stem-like cells. Dev Dyn. 2007; 236:3297–3308. [PubMed: 18000980]
15. Lenart B, Kintner DB, Shull GE, Sun D. Na-K-Cl cotransporter-mediated intracellular Na^+ accumulation affects Ca^{2+} signaling in astrocytes in an in vitro ischemic model. J Neurosci. 2004; 24:9585–9597. [PubMed: 15509746]
16. Rocha-Gonzalez HI, Mao S, Alvarez-Leefmans FJ. Na^+,K^+,$2Cl^-$ cotransport and intracellular chloride regulation in rat primary sensory neurons: thermodynamic and kinetic aspects. J Neurophysiol. 2008; 100:169–184. [PubMed: 18385481]
17. Kiedrowski L. N-methyl-D-aspartate excitotoxicity: relationships among plasma membrane potential, Na(+)/Ca(2+) exchange, mitochondrial Ca(2+) overload, and cytoplasmic concentrations of Ca(2+), H(+), and K(+). Mol Pharmacol. 1999; 56:619–632. [PubMed: 10462550]
18. Su G, Haworth RA, Dempsey RJ, Sun D. Regulation of Na^+-K^+-Cl^- cotransporter in primary astrocytes by dibutyryl cAMP and high $[K^+]_o$. Am J Physiol Cell Physiol. 2000; 279:C1710–C1721. [PubMed: 11078685]
19. Flemmer AW, Gimenez I, Dowd BF, Darman RB, Forbush B. Activation of the Na-K-Cl cotransporter NKCC1 detected with a phospho-specific antibody. J Biol Chem. 2002; 277:37551–37558. [PubMed: 12145305]
20. Su G, Kintner DB, Flagella M, Shull GE, Sun D. Astrocytes from Na(+)-K(+)- Cl(−) cotransporter-null mice exhibit absence of swelling and decrease in EAA release. Am J Physiol Cell Physiol. 2002; 282:C1147–C1160. [PubMed: 11940530]
21. Sung KW, Kirby M, McDonald MP, Lovinger DM, Delpire E. Abnormal GABAA receptor-mediated currents in dorsal root ganglion neurons isolated from Na-K-2Cl cotransporter null mice. J Neurosci. 2000; 20:7531–7538. [PubMed: 11027211]
22. Hirose Y, Berger MS, Pieper RO. p53 effects both the duration of G2/M arrest and the fate of temozolomide-treated human glioblastoma cells. Cancer Res. 2001; 61:1957–1963. [PubMed: 11280752]
23. Sontheimer H. An unexpected role for ion channels in brain tumor metastasis. Exp Biol Med (Maywood). 2008; 233:779–791. [PubMed: 18445774]
24. Haas BR, Sontheimer H. Inhibition of the Sodium-Potassium-Chloride Cotransporter Isoform-1 reduces glioma invasion. Cancer Res. 2010; 70:5597–5606. [PubMed: 20570904]
25. Habela CW, Ernest NJ, Swindall AF, Sontheimer H. Chloride accumulation drives volume dynamics underlying cell proliferation and migration. J Neurophysiol. 2009; 101:750–757. [PubMed: 19036868]
26. Yamada J, Okabe A, Toyoda H, Kilb W, Luhmann HJ, Fukuda A. Cl^- uptake promoting depolarizing GABA actions in immature rat neocortical neurones is mediated by NKCC1. J Physiol. 2004; 557:829–841. [PubMed: 15090604]
27. Ge S, Goh EL, Sailor KA, Kitabatake Y, Ming GL, Song H. GABA regulates synaptic integration of newly generated neurons in the adult brain. Nature. 2006; 439:589–593. [PubMed: 16341203]
28. Chimote AA, Adragna NC, Lauf PK. Ion transport in a human lens epithelial cell line exposed to hyposmotic and apoptotic stress. J Cell Physiol. 2010; 223:110–122. [PubMed: 20049853]
29. Olsen ML, Schade S, Lyons SA, Amaral MD, Sontheimer H. Expression of voltage-gated chloride channels in human glioma cells. J Neurosci. 2003; 23:5572–5582. [PubMed: 12843258]
30. Ernest NJ, Weaver AK, Van Duyn LB, Sontheimer HW. Relative contribution of chloride channels and transporters to regulatory volume decrease in human glioma cells. Am J Physiol Cell Physiol. 2005; 288:C1451–C1460. [PubMed: 15659714]
31. Gagnon KB, Adragna NC, Fyffe RE, Lauf PK. Characterization of glial cell K-Cl cotransport. Cell Physiol Biochem. 2007; 20:121–130. [PubMed: 17595522]
32. Nico B, Mangieri D, Tamma R, Longo V, Annese T, Crivellato E, Pollo B, Maderna E, Ribatti D, Salmaggi A. Aquaporin-4 contributes to the resolution of peritumoural brain oedema in human glioblastoma multiforme after combined chemotherapy and radiotherapy. Eur J Cancer. 2009; 45:3315–3325. [PubMed: 19836227]
33. Numata T, Sato K, Okada Y, Wehner F. Hypertonicity-induced cation channels rescue cells from staurosporine-elicited apoptosis. Apoptosis. 2008; 13:895–903. [PubMed: 18478334]

34. Subramanyam M, Takahashi N, Hasegawa Y, Mohri T, Okada Y. Inhibition of protein kinase Akt1 by apoptosis signal-regulating kinase-1 (ASK1) is involved in apoptotic inhibition of regulatory volume increase. J Biol Chem. 2010; 285:6109–6117. [PubMed: 20048146]
35. Panayiotidis MI, Bortner CD, Cidlowski JA. On the mechanism of ionic regulation of apoptosis: would the Na^+/K^+-ATPase please stand up? Acta Physiol (Oxf). 2006; 187:205–215. [PubMed: 16734757]
36. Xiao AY, Wei L, Xia S, Rothman S, Yu SP. Ionic mechanism of ouabain-induced concurrent apoptosis and necrosis in individual cultured cortical neurons. J Neurosci. 2002; 22:1350–1362. [PubMed: 11850462]
37. Beck J, Lenart B, Kintner DB, Sun D. Na-K-Cl cotransporter contributes to glutamate-mediated excitotoxicity. J Neurosci. 2003; 23:5061–5068. [PubMed: 12832529]
38. Dowd BF, Forbush B. PASK (proline-alanine-rich STE20-related kinase), a regulatory kinase of the Na-K-Cl cotransporter (NKCC1). J Biol Chem. 2003; 278:27347–27353. [PubMed: 12740379]
39. Gagnon KB, England R, Delpire E. Characterization of SPAK and OSR1, regulatory kinases of the Na-K-2Cl cotransporter. Mol Cell Biol. 2006; 26:689–698. [PubMed: 16382158]
40. Kahle KT, Rinehart J, Lifton RP. Phosphoregulation of the Na-K-2Cl and K-Cl cotransporters by the WNK kinases. Biochim Biophys Acta. 2010; 1802:1150–1158. [PubMed: 20637866]
41. Vitari AC, Deak M, Morrice NA, Alessi DR. The WNK1 and WNK4 protein kinases that are mutated in Gordon's hypertension syndrome phosphorylate and activate SPAK and OSR1 protein kinases. Biochem J. 2005; 391:17–24. [PubMed: 16083423]
42. Gagnon KB, England R, Delpire E. Characterization of SPAK and OSR1, regulatory kinases of the Na-K*2Cl cotransporter. Mol Cell Biol. 2006; 26:689–698. [PubMed: 16382158]
43. Flemmer AW, Monette MY, Djurisic M, Dowd B, Darman R, Gimenez I, Forbush B. Phosphorylation state of the Na^+-K^+-Cl^- cotransporter (NKCC1) in the gills of Atlantic killifish (Fundulus heteroclitus) during acclimation to water of varying salinity. J Exp Biol. 2010; 213:1558–1566. [PubMed: 20400641]
44. Park JA, Joe YA, Kim TG, Hong YK. Potentiation of antiglioma effect with combined temozolomide and interferon-beta. Oncol Rep. 2006; 16:1253–1260. [PubMed: 17089046]
45. Beier D, Rohrl S, Pillai DR, Schwarz S, Kunz-Schughart LA, Leukel P, Proescholdt M, Brawanski A, Bogdahn U, Trampe-Kieslich A, Giebel B, Wischhusen J, Reifenberger G, Hau P, Beier CP. Temozolomide preferentially depletes cancer stem cells in glioblastoma. Cancer Res. 2008; 68:5706–5715. [PubMed: 18632623]

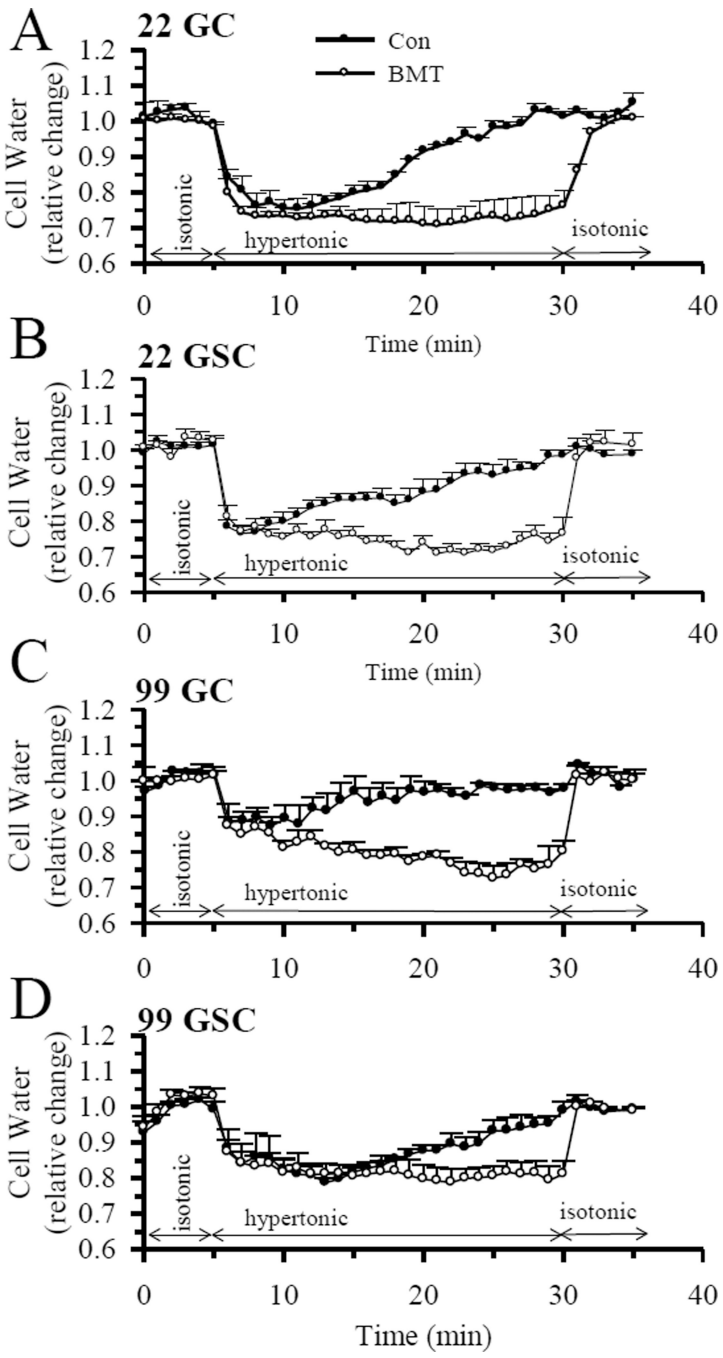

Figure 1. NKCC1-mediated regulatory volume increase (RVI)

The fluorescent dye calcein was used to measure cell water content and relative cell volume as described in Methods. Cells were exposed to isotonic HEPES-MEM (310 mOsm, 5 min), hypertonic HEPES-MEM (370 mOsm, 25 min), and isotonic HEPES-MEM (5 min). In the BMT studies, 10 μM BMT was added 30 min prior to the isotonic exposure. **A**. GC (#22). **B**. GSC (#22). **C**. GC (#99). **D**. GSC (#99). Data are means ± SEM. n = 4–7.

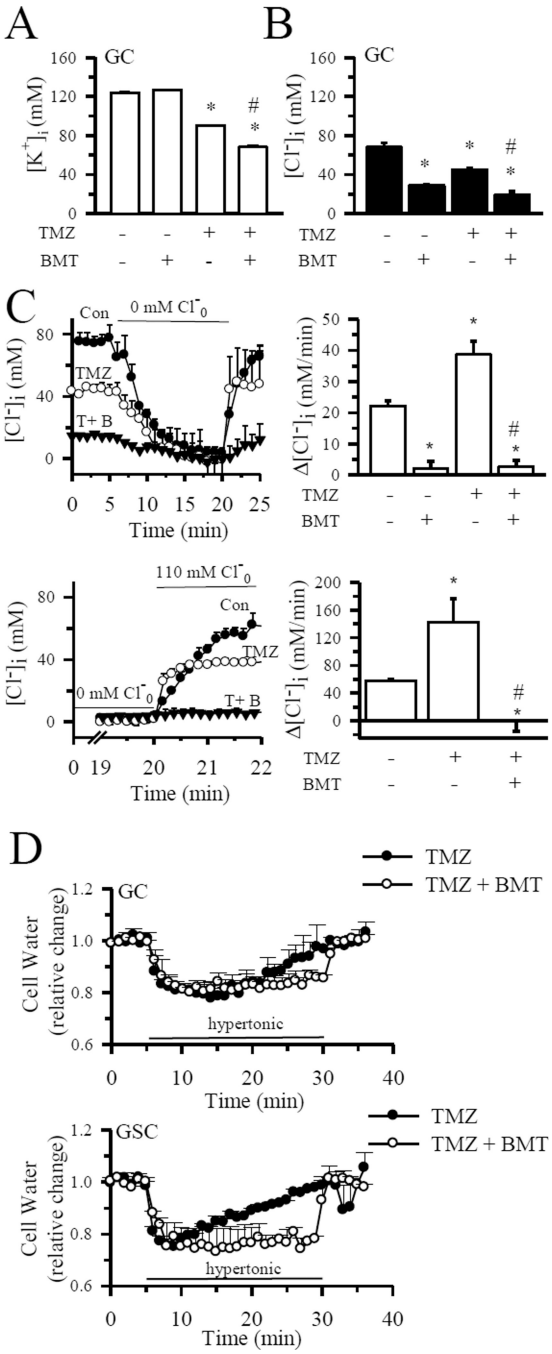

Figure 2. Inhibition of NKCC1 activity accelerates TMZ-induced loss of K^+_i and Cl^-_i

A. $[K^+]_i$ in GC (#22) was determined using the fluorescent probe PBFI following 4 h of treatment with control medium, 10 μM BMT, 100 μM TMZ or TMZ plus 10 μM BMT. Data are means ± SEM, n = 3. * $p < 0.05$ vs. Con, # $p < 0.05$ vs. TMZ. **B**. $[Cl^-]_i$ in GC (#22) exposed to control medium, 10 μM BMT, 100 μM TMZ, or TMZ plus 10 μM BMT. Data are means ± SEM, n = 3–6. * $p < 0.05$ vs. Con, # $p < 0.05$ vs. TMZ. **C. Upper left panel:** Changes of $[Cl^-]_i$ in GC in normal isotonic buffer, followed by exposure to 0 mM Cl^- for 15 min and subsequent exposure to normal isotonic buffer. Images were acquired every 1 min. **Upper right panel:** Summary data of the NKCC1-mediated Cl^-_i replenishment rate

following 0 mM Cl^- exposure were shown. Slopes were calculated between 0 and 1 min of Cl^-_i replenishment. **Lower left panel:** Experimental protocol was identical to upper panel. Images were collected every 10 sec beginning at 14 min of 0 mM Cl^- exposure. Cells were either treated with 100 μM TMZ or 100 μM TMZ and 10 μM BMT for 4 h. **Lower right panel:** Summary data of Cl^-_i replenishment slopes that were calculated between 0 and 10 sec of Cl^-_i replenishment. Drugs were present for the entire experiment. Data are means ± SEM, n = 3–6. * $p < 0.05$ vs. Con, # $p < 0.05$ vs. TMZ. **D**. NKCC1-mediated RVI remains active in TMZ treatment. RVI was determined in either GC (#22) or GSC (#22) after 4 h of treatment with 100 μM TMZ or TMZ plus 10 μM BMT. Data are means ± SEM. n = 3.

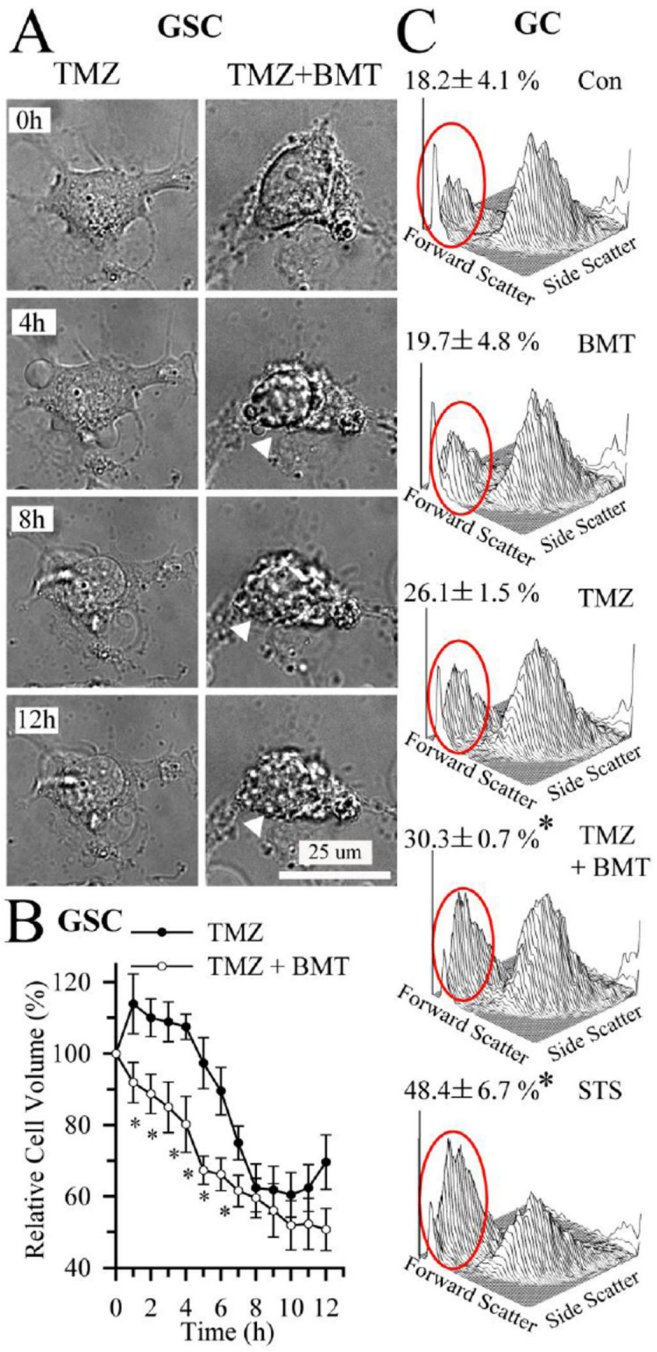

Figure 3. Blocking NKCC1 activity accelerates AVD after TMZ treatment

A. Time-lapse DIC images were used to measure changes in cell volume in GSC (#22). Cultures were treated with TMZ (500 μM) or TMZ + BMT (10 μM) and representative images of cells at times 0, 4, 8, and 12 h are shown. Inhibition of NKCC1 with BMT accelerated AVD, as evident by the loss of processes, and cell body shrinkage (arrowhead). **B.** Summary data of relative cell volume changes. Data are means ± SEM. n = 8–9. * $p < 0.05$ vs. corresponding TMZ. **C.** GC (#22) were exposed to normal medium (Con), Con + 10 μM BMT, 500 μM TMZ, 500 μM TMZ + 10 μM BMT or 4 μM STS for 4 h. Cell size was examined by flow cytometry using a FSC versus SSC 3D plot. 4 μM STS-treated GC were

used as a positive control for AVD. Red circle: shrunken population of cells in the 3D plots. Data are means ± SD. n = 3. * $p < 0.05$. vs. Con.

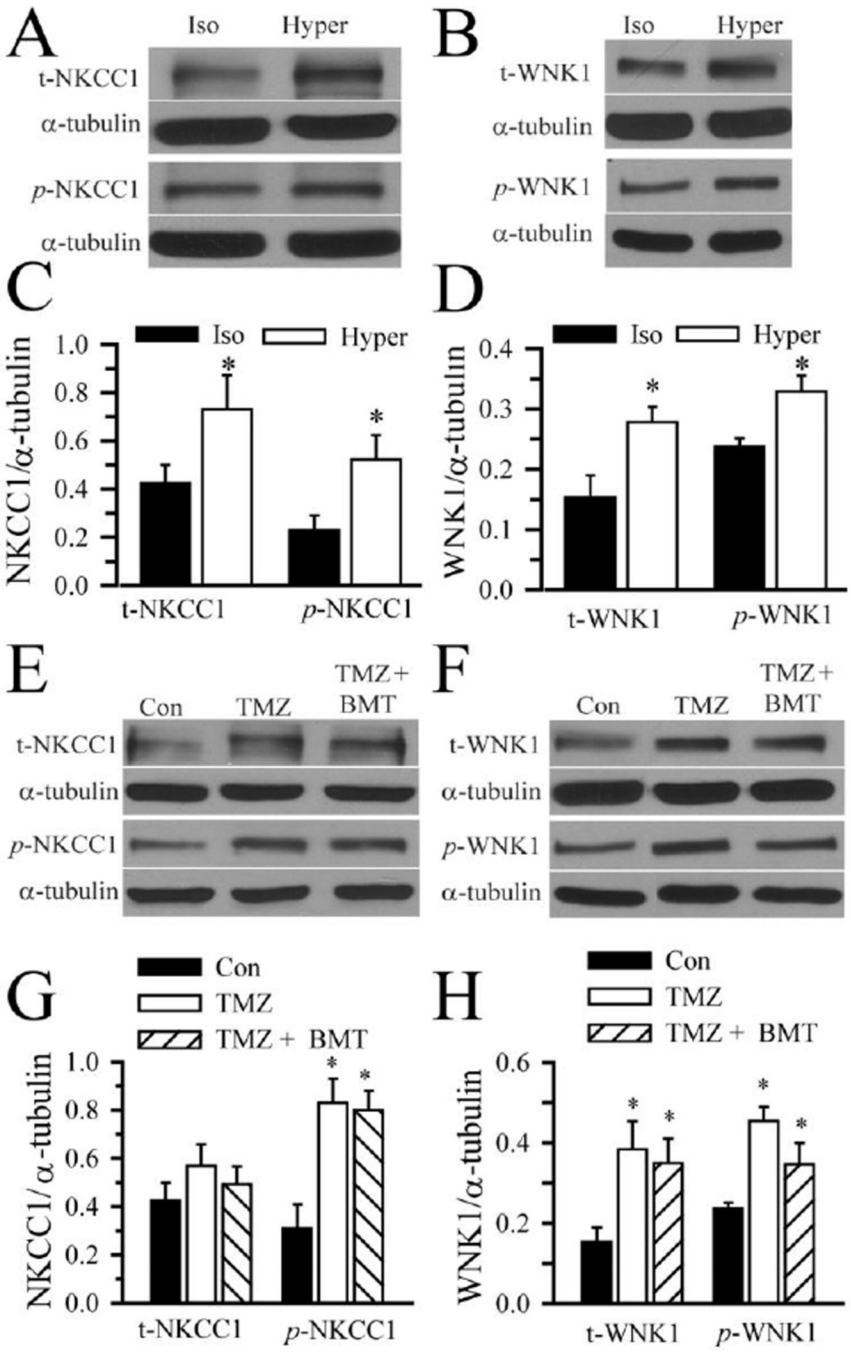

Figure 4. Activation of NKCC1 and WNK1 following osmotic stress and TMZ treatment

A–D. GC (#22) were exposed to isotonic (310 mOsm) or hypertonic HEPES-MEM (370 mOsm) for 25 min. Expression of total NKCC1, total WNK1, phosphorylated NKCC1 (*p*-NKCC1), and phosphorylated WNK1 (*p*-WNK1) were evaluated by immunoblotting. **A, B**. Representative immunoblots showing expression of t-NKCC1, *p*-NKCC1, t-WNK1 and *p*-WNK1 protein under isotonic and hypertonic conditions. **C, D**. Summary data of immunoblotting. NKCC1/α-tubulin ratio (either t-NKCC1 or *p*-NKCC1) and WNK1/α-tubulin ratio (either t-WNK1 or *p*-WNK1) were calculated. Data are mean ± SD, n = 3–4, * $p < 0.05$ vs. Iso. **E–H**. GC (#22) were exposed to isotonic medium (Con), 100 μM TMZ, or

TMZ plus 10 μM BMT for 4 h. Expression of t-NKCC1, t-WNK1, *p*-NKCC1, and *p*-WNK1 were evaluated by immunoblotting. **E, F**. Representative immunoblots. The pWNK1 control sample in F is the same isotonic control sample in panel B. **G, H**. Summary data of immunoblotting. NKCC1/α-tubulin ratio (either t-NKCC1 or *p*-NKCC1) and WNK1/α-tubulin ratio (either t-WNK1 or *p*-WNK1) were calculated. Data are mean ± SD. n = 3–4, * $p < 0.05$ vs. Con.

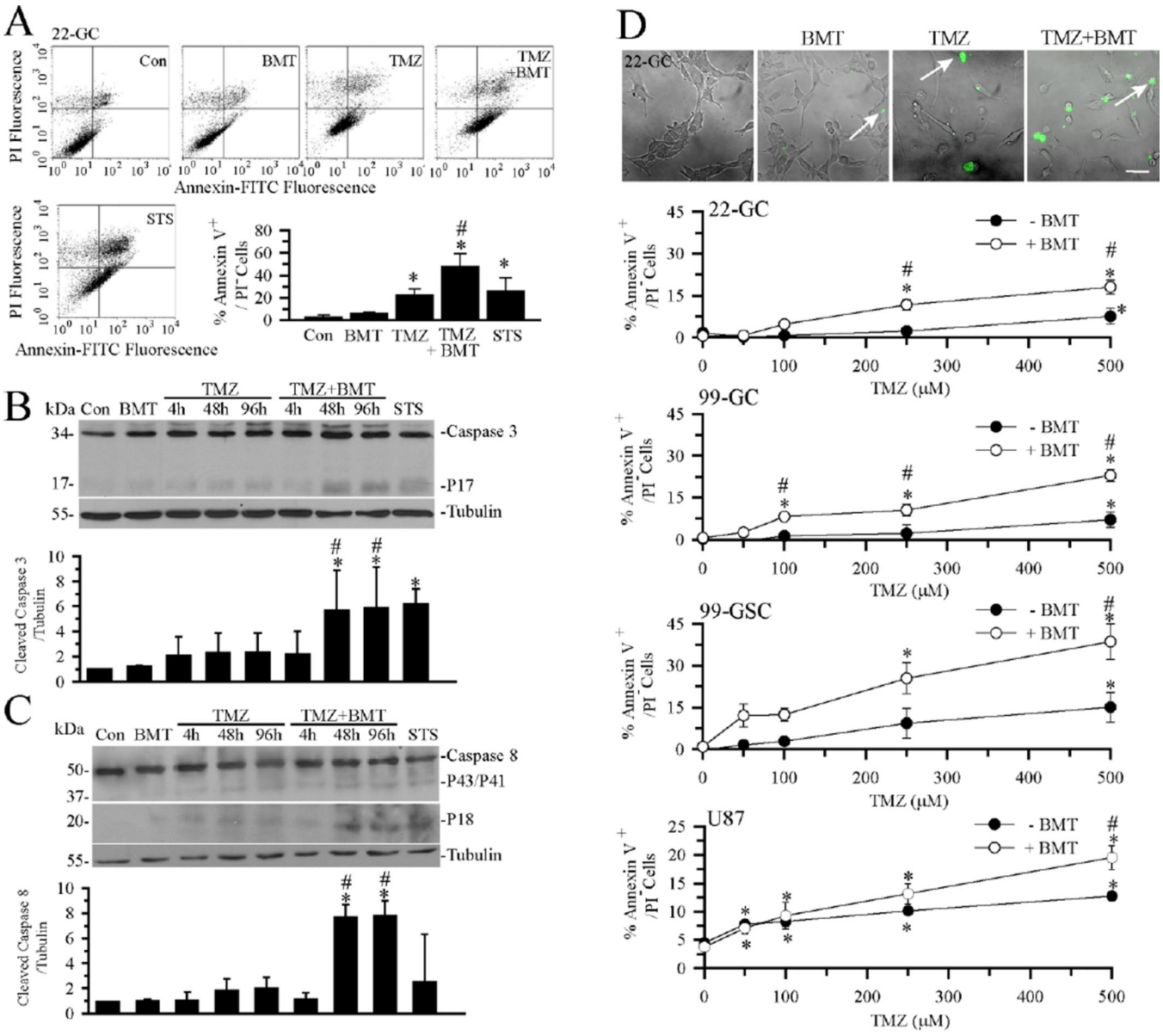

Figure 5. Blocking NKCC1 activity enhances TMZ-mediated apoptosis

A. Apoptosis in GC (#22) was assessed by Annexin-V vs. PI staining in flow cytometry. GC were exposed to normal medium (Con), Con + 10 μM BMT, 500 μM TMZ, 500 μM TMZ + 10 μM BMT or 4 μM STS for 4 h. Representative dot-plots show viable cells (lower left quadrant), early apoptotic cells (lower right quadrant), and late apoptotic or necrotic cells (upper right quadrant). Bottom right hand panel: Summary data of cells with Annexin-V positive and PI-negative staining. Data are means ± SD, n = 3. * $p < 0.05$ vs. Con. # $p < 0.05$ vs. TMZ. **B, C.** Representative immunoblots and summary data of activated caspase-3 and caspase-8 in GC (#22) following exposure to normal medium (Con), Con + 10 μM BMT, 100 μM TMZ, 500 μM TMZ + 10 μM BMT or 4 μM STS for 4 h. Data are means ± SD, n = 3. * $p < 0.05$ vs. Con. # $p < 0.05$ vs. correspondent 100 μM TMZ. **D**. BMT sensitized GC and GSC to TMZ-induced phosphatidylserine externalization. **Top panel:** Early apoptotic cells (GC #22) are revealed by FITC-conjugated Annexin staining (arrow) under conditions of Con, Con + 10 μM BMT, 500 μM TMZ, or 500 μM TMZ + 10 μM BMT for 48 h. Scale

bar = 50 μM. **Lower panels**: Summary data of TMZ dose-response curves at 48 h in GC (#22), GC (#99), GSC (#99), or U87MG. Data are means ± SEM. n = 3–6. * $p < 0.05$ vs. 0 mM TMZ, # $p < 0.05$ vs. corresponding BMT.

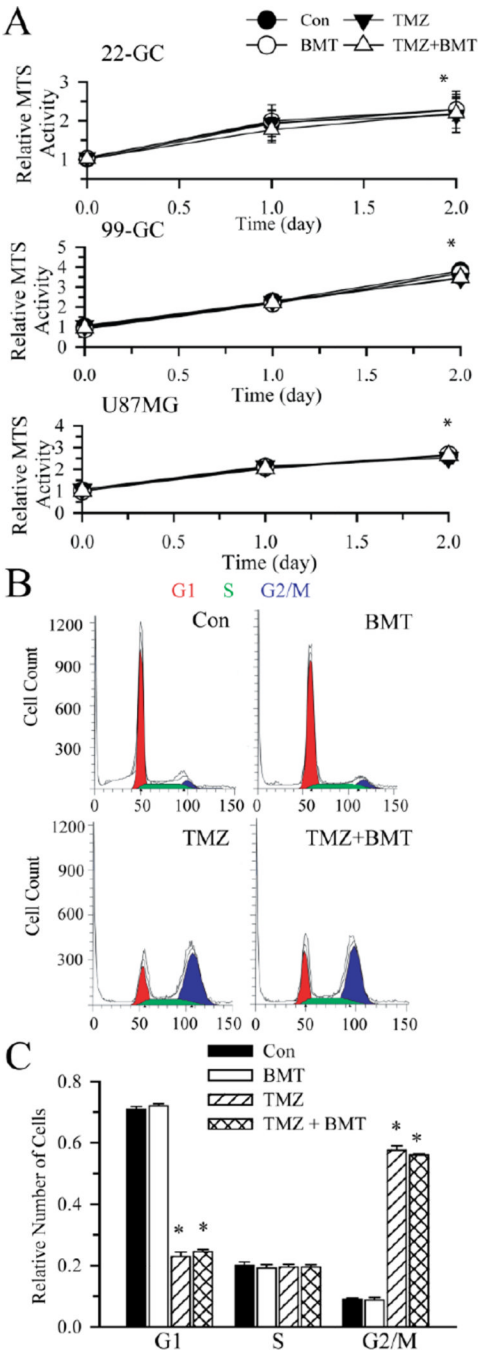

Figure 6. Cell proliferation and cell cycle arrest in the presence of TMZ

A. Graphs of relative MTS activity in cells under each condition. Data are means ± SD. n = 3. * $p < 0.05$ vs. Con. **B.** Flow cytometric analysis of cell cycle distribution of GC (#22) cells treated with vehicle (DMSO), 10 μM BMT, 250 μM TMZ, 250 μM TMZ + 10 μM BMT for 96 h. The G1(red), S (Green), and G2/M (blue) phases are indicated. **C.** A summary graph of percent GC cells in each phase of cell cycle. Data are means ± SEM. n = 3. * $p < 0.05$ vs. Con.

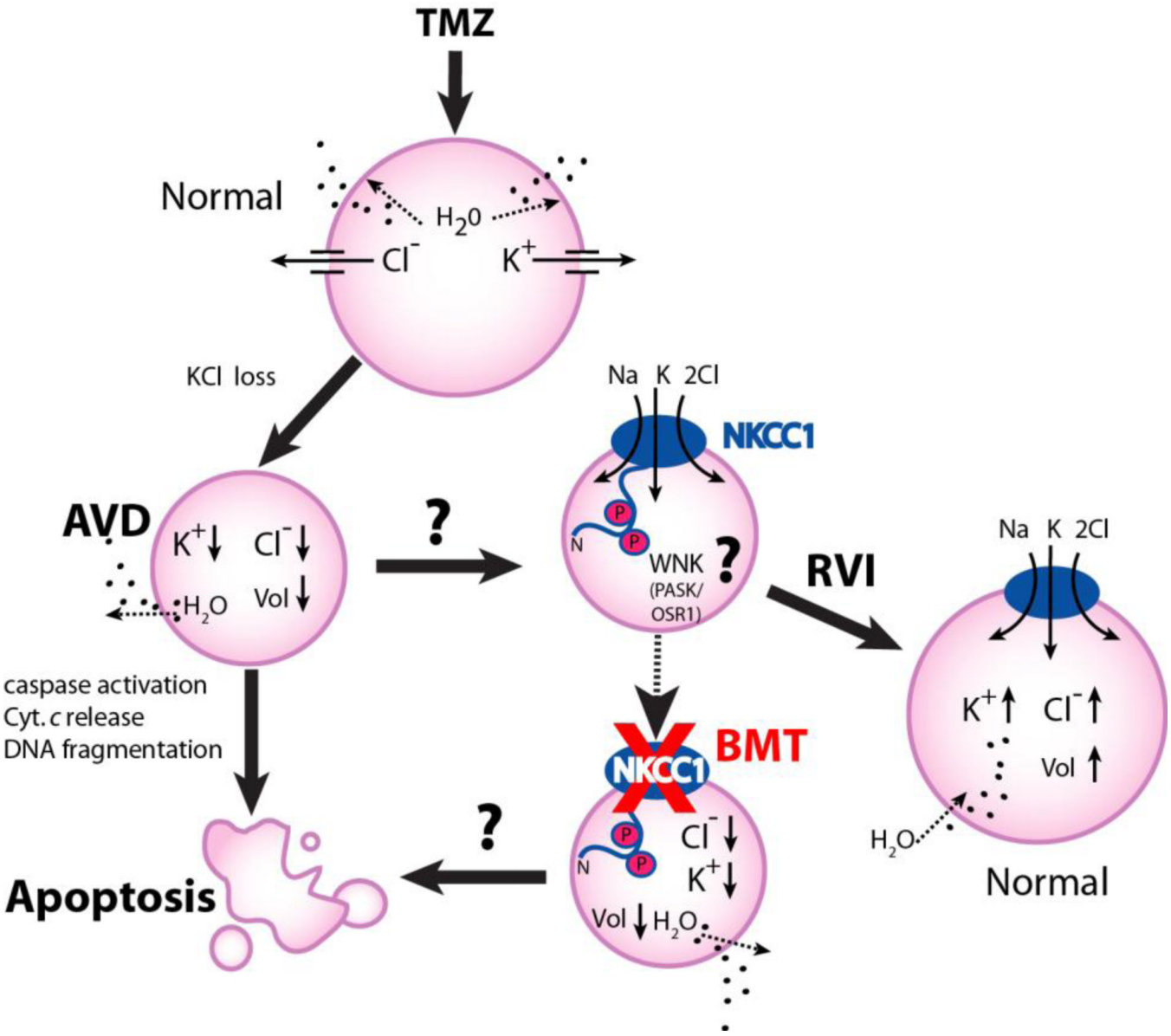

Figure 7. A schematic model of NKCC1 in TMZ-mediated apoptosis

TMZ triggers loss of K^+_i, Cl^-_i and apoptotic volume decrease (AVD), and leads to apoptotic cell death in glioblastoma cancer cells. NKCC1 activity may be stimulated via the novel Cl^-/volume-sensitive regulatory kinases WNK-mediated signaling transduction pathway in response to TMZ. Activation of NKCC1 in TMZ-treated cells accumulate Na^+_i, K^+_i, and Cl^-_i and obligated water molecules (regulatory volume increase, RVI) to counteract ionic dysregulation and AVD and promote cell survival. Inhibition of NKCC1 activity with BMT would facilitate loss of K^+_i, Cl^-_i and AVD, thus augments glioma cells to TMZ-mediated apoptosis.